Disappearance of Nodal Gap across the Insulator-Superconductor Transition in a Copper-Oxide Superconductor

Yingying Peng[1], Jianqiao Meng[1], Daixiang Mou[1], Junfeng He[1], Lin Zhao[1], Yue Wu[1], Guodong Liu[1], Xiaoli Dong[1], Shaolong He[1], Jun Zhang[1], Xiaoyang Wang[2], Qinjun Peng[2], Zhimin Wang[2], Shenjin Zhang[2], Feng Yang[2], Chuangtian Chen[2], Zuyan Xu[2], T. K. Lee[3] and X. J. Zhou[1,*]

[1]*National Laboratory for Superconductivity, Beijing National Laboratory for Condensed Matter Physics, Institute of Physics, Chinese Academy of Sciences, Beijing 100190, China*

[2]*Technical Institute of Physics and Chemistry, Chinese Academy of Sciences, Beijing 100190, China*

[3]*Institute of Physics, Academia Sinica, Nankang, Taipei 11529, Taiwan*

(Dated: February 13, 2013)

The parent compound of the copper-oxide high temperature superconductors is a Mott insulator. Superconductivity is realized by doping an appropriate amount of charge carriers. How a Mott insulator transforms into a superconductor is crucial in understanding the unusual physical properties of high temperature superconductors and the superconductivity mechanism. Systematic investigations of the electronic structure in the lightly-doped region, especially across the insulator-superconductor transition are necessary but so far have not reached a consistent picture. In this paper, we report high resolution angle-resolved photoemission measurement on heavily underdoped $Bi_2Sr_{2-x}La_xCuO_{6+\delta}$ system. The electronic structure of the lightly-doped samples exhibit a number of characteristics: existence of an energy gap along the (0,0)-(π,π) nodal direction, d-wave-like anisotropic energy gap along the underlying Fermi surface, and coexistence of coherence peak and a broad hump in the photoemission spectra. Our results reveal a clear insulator-superconductor transition at a critical doping level of $\sim$0.10 where the nodal energy gap approaches zero, the three-dimensional antiferromagnetic order disappears, and superconductivity starts to emerge. These observations clearly signal a close connection between the nodal gap, antiferromagnetic insulating phase, and high temperature superconductivity. They point to the importance of combining the electron correlation, antiferromagnetism and strong electron-phonon coupling in understanding high temperature superconductors in the very underdoped region.

The parent compound of the copper-oxide superconductors is an antiferromagnetic Mott insulator; doping of charge carriers into the parent compound leads to an insulator-metal transition and the emergence of high temperature superconductivity[1]. In the superconducting state, predominantly *d*-wave superconducting gap is well-established with a zero gap along the nodal direction[2]. In the normal state of the underdoped superconducting region, anisotropic pseudogap appears with a zero gap along the nodal direction[3]. A particular yet important region exists between the parent compound and the superconducting region, i.e., a lightly-doped region where, upon a slight doping, the three dimensional antiferromagnetic order is rapidly suppressed and an insulator-metal transition occurs. What is the main reason for the antiferromagnetic phase remain insulating after being doped? What is the electronic characteristics of this peculiar lightly-doped region? How is the electronic

structure of this particular region connected to the pseudogap and superconducting gap in the underdoped superconducting region? Investigation of this lightly-doped region is critical in understanding how a Mott insulator can transform into a *d*-wave superconductor, and the origin of the pseudogap and its relationship with the superconducting gap[4, 5].

In this paper we report angle-resolved photoemission (ARPES) measurements on the electronic structure evolution with doping in $Bi_2(Sr_{2-x}La_x)CuO_{6+\delta}$ (La-Bi2201) system focusing on the lightly-doped region and the insulator-superconductor transition. Our super-high resolution ARPES experiments reveal an insulator-superconductor transition at a critical doping level of $p{\sim}0.10$. In the lightly-doped region (p=0−0.10), the photoemission spectra are characterized by the coexistence of a coherence peak and a broad hump consistent with a polaronic behavior. Moreover, a fully-opened *d*-wave-like anisotropic energy gap is observed which is offset by an energy gap along the (0,0)-(π,π) nodal direction. The nodal gap decreases with increasing doping and approaches zero at a critical doping level of $p{\sim}0.1$, where the three-dimensional (3D) antiferromagnetic order vanishes and superconductivity starts to emerge[6]. In addition, a smooth transition from the energy gap in the lightly-doped region to the pseudogap in the underdoped superconducting region is observed. These observations indicate a close relationship between the nodal energy gap, antiferromagnetic insulating phase and superconductivity. They will shed important light on the origin of the pseudogap in high temperature superconductors, and point to the importance of combining the electron correlation, antiferromagnetism and strong electron-phonon coupling in understanding the electronic structure of the lightly-doped and underdoped regions.

The ARPES measurements were carried out on our vacuum ultraviolet (VUV) laser-based angle-resolved photoemission system with advantages of high photon flux, enhanced bulk sensitivity and super-high energy and momentum resolution[7]. The photon energy is 6.994 eV with a bandwidth of 0.26 meV. We set the energy resolution of the electron energy analyzer (Scienta R4000) at 1.5 meV, giving rise to an overall instrumental energy resolution of 1.52 meV. The angular resolution is ∼0.3°, corresponding to a momentum resolution of $\sim 0.004 \mathring{A}^{-1}$. The $Bi_2Sr_{2-x}La_xCuO_{6+\delta}$ (La-Bi2201) single crystals were grown by the traveling solvent floating zone method[8]. We obtained various dopings by changing the La concentration and post-annealing under different temperatures and atmospheres (see Supplementary Materials): the sample with the hole concentration p=0.03 has a composition of x=1.05 while all the other samples with hole concentrations of 0.04, 0.055, 0.07,

0.08, 0.10 and 0.105 have the same composition with x=0.84 but annealed under different conditions. The samples with hole concentrations p of 0.03, 0.04, 0.055, 0.07 and 0.08 are non-superconducting. The p=0.10 sample is superconducting with a transition temperature T_c∼3 K, near the border of nonsuperconductor-to-superconductor transition. The p=0.105 sample shows a T_c of 12 K. The samples were cleaved *in situ* and measured under ultrahigh vacuum better than 4×10^{-11} Torr.

Figure 1 shows the doping evolution of the underlying Fermi surface across the non-superconductor-superconductor transition and indications of the nodal energy gap observed for the lightly-doped La-Bi2201 samples. As seen from Fig. 1(a-d), in the lightly-doped samples, the spectral weight distribution dominates near the (π/2,π/2) nodal region and then spreads towards the (π,0) anti-nodal region with increasing doping. As commonly used before, we denote the high intensity contour in the spectral weight distribution as the "underlying Fermi surface"[9] although in principle, a strict Fermi surface refers to the lotus of momentum without an energy gap. The photoemission spectra (energy distribution curves, EDCs) along the underlying Fermi surface are displayed in Fig. 1(e, g, i, k) for different doping levels, with their corresponding symmetrized EDCs shown in Fig. 1(f, h, j and l), respectively. The EDC symmetrization is an empirical and intuitive way to examine the existence of an energy gap by removing the Fermi distribution function from the original ARPES data[10]. As seen from Fig. 1e and 1f, with very low doping of p=0.03, only a broad hump feature dominates the measured spectra. It disperses toward low binding energy, reaches its minimum around 200 meV along the nodal direction and then turns back. The spectral weight near the Fermi level E_F is strongly suppressed for this lightly-doped sample and there is apparently a gap opening. Further increase of the doping to p=0.055 results in an emergence of a coherence peak near the Fermi level which coexists with the broad hump structure (Fig. 1g). A close inspection reveals an energy gap for the coherence peak along the entire underlying Fermi surface, including the nodal region (Fig. 1h). When the doping level reaches p=0.08, the coherence peak becomes prominent. In the mean time, the broad hump gets weaker but remains visible (Fig. 1i). The energy gap opening is clear along the entire underlying Fermi surface(Fig. 1j). Eventually, when the doping level becomes p=0.10, the coherence peak gets sharp and the broad hump remains discernable (Fig. 1k). But in this case, no indication of an energy gap opening is observed near the nodal region (Fig. 1l). However, there are clear indications of gap opening in the EDCs far away from

the nodal region. This is consistent with the observation of the Fermi arc in underdoped superconducting samples[11–13].

Figure 2 focuses on the nodal gap and its detailed doping evolution. Fig. 2(a-g) shows doping evolution of the band structure along the nodal direction. The Fermi distribution function is divided out from these data to facilitate the revelation of the energy gap near the Fermi level. Original EDCs for the La-Bi2201 samples with different doping levels are shown in Fig. 2h on the underlying Fermi surface along the nodal direction, with their corresponding symmetrized EDCs shown in Fig. 2i. From the raw data (Fig. 2(a-g)), it is clear that, with increasing doping, the spectral weight transfers from high binding energy to lower binding energy. For the p=0.03 sample, the spectral weight near E_F is strongly depleted (Fig. 2a) and the nodal EDC is characterized by a prominent broad hump near 250 meV. A slight increase of the doping level to 0.04 brings a significant amount of spectral weight towards low binding energy and a weak coherence peak emerges near the Fermi level (Fig. 2b and 2h). Further doping brings more spectral weight to the Fermi level with the broad hump structure remaining while the coherence peak near the Fermi level becomes sharper with increasing doping. The relative spectral weight increase of the coherence peak with increasing doping is shown in the inset of Fig. 2h (red circles). Similar trend was observed before in other cuprates[14, 15]. We note that, compared with the previous results[16, 17], this is the first time one can observe clear coherence peaks below the doping level of p=0.10 in Bi2201 and a coexistence of peak-dip-hump structure for such low doping samples. This is mainly due to sample quality improvement and the utilization of super-high resolution of our laser ARPES measurements. The observation of a clear coherence peak near the Fermi level makes it possible to precisely determine the energy gap. As shown in the symmetrized nodal EDCs in Fig. 2i, whereas the symmetrized EDC of the p=0.03 sample becomes featureless near E_F, there is a clear indication of nodal gap opening in the samples with doping of p=0.04 to p=0.08. Such a nodal gap is closed for the p=0.10 and p=0.105 samples. As shown in the inset of Fig. 2h, the nodal gap drops monotonically with increasing doping till the doping level of 0.10 which just becomes superconducting with a T_c around 3 K.

In order to understand the origin of the nodal gap in the lightly doped samples, it is important to investigate its temperature dependence. Fig. 3 shows the temperature evolution of the band structure and the nodal gap in a typical La-Bi2201 sample with a doping level of 0.055. The measured data are divided by the Fermi distribution function

(Fig. 3a) in order to visually inspect the energy gap as well as the possible features above the Fermi level. There is clearly a spectral weight suppression near the Fermi level for all the temperatures we have covered. This indicates that the nodal gap persists in the entire temperature range up to 300 K, close to the temperature of the possible pseudogap as determined by the NMR meausrements[6]. From the original EDCs on the underlying Fermi surface along the nodal direction (Fig. 3b), one can see that, with increasing temperature, the coherence peak gets weak and becomes indiscernible above 150 K, while the high energy hump shows a slight change with temperature. The corresponding EDCs after dividing out the Fermi distribution functions (Fig. 3c) exhibit a dip near the Fermi level, which together with the spectral distribution in the original data (Fig. 3a), indicate that the gap below and above the Fermi level is nearly symmetric. This justifies the procedure in symmetrizing EDCs to extract the energy gap in the paper. Fig. 3d shows symmetrized EDCs on the underlying Fermi surface along the nodal direction; one can also see the persistence of the nodal gap till high temperatures. We do not show EDCs above 150 K in Fig. 3(b-d) because the disappearance of the coherence peak at high temperatures makes it difficult to quantitatively determine the gap size.

To investigate the momentum dependence of the energy gap in the lightly-doped La-Bi2201, we have measured various momentum cuts along the underlying Fermi surface, picked up the EDCs along the underlying Fermi surface like in Fig. 1(e, g, i ,k), and extracted the gap size from the peak position of the symmetrized EDCs like in Fig. 1(f, h, j, l). The obtained gap size as a function of momentum is shown in Fig. 4(a, b, c, d, e) for the La-Bi2201 samples with doping levels at 0.04, 0.055, 0.07, 0.08 and 0.10, respectively. Also shown in Fig. 4(f, g, h, i, j, k,) is the position of the high energy hump as a function of momentum for the La-Bi2201 samples at different doping levels. It is clear that the gap is anisotropic that increases when the momentum moves from the nodal to the antinodal regions. For comparison, we also plotted an offset *d*-wave gap form $\Delta=\Delta_0\cos(2\Phi)+\Delta_N$ with Δ_N representing the nodal gap (solid dashed lines in Fig. 4(a-d)) and one can see that the measured data basically follow such a simple form in the samples with doping p=0.03$\sim$0.08. This is consistent with the previous report that *d*-wave like gap is observed in the parent compound $Ca_2CuO_2Cl_2$[18], insulating $Bi_2Sr_2CaCu_2O_{8+\delta}$ (Bi2212)[19], heavily underdoped Bi2212[20] and underdoped $(La_{2-x}Sr_x)CuO_4$[21]. The presence of the nodal gap indicates that the underlying Fermi surface is fully gapped for these samples. At the critical

doping $p\sim0.10$ where superconductivity emerges, it shows zero gap near the nodal region which is consistent with the "Fermi arc" picture in the pseudogap state of other copper-oxide superconductors[11, 12]. It is interesting to note that the broad hump structure also exhibits anisotropic momentum dependence with its position following a form $P_h=P_{h0}\cos(2\Phi)+P_{hN}$ with P_{hN} representing the hump position along the nodal direction (Fig. 4(f-k)). The hump structure exhibits a minimum in binding energy along the nodal direction and its position decreases with the increase of doping levels. The similar momentum dependence of both the energy gap and the hump, and their similar doping dependence, suggest that they are intimately related, as will be discussed more below. Fig. 4l illustrates the evolution of the energy gap and its relation with the three-dimensional antiferromagnetism (AF) and superconductivity[6]. At a critical doping level of $p\sim0.10$, the nodal gap approaches to zero, the three dimensional antiferromagnetism vanishes, and superconductivity (SC) starts to emerge.

Our observation of the nodal gap, and hence a fully-gapped underlying Fermi surface in the lightly-doped La-Bi2201 samples (p=0−0.10) indicates they have an insulating ground state. This is in a good correspondence to the transport measurements where the insulating behavior is observed until p=0.08 in the resistivity-temperature dependence (See Fig. S1a in Supplementary Materials). Previous optical measurements also indicated a gap opening with the transition from insulator to metal near a doping of $p\sim0.10$ in La-Bi2201[22]. The temperature dependence of the resistivity fits well with the model of two-dimensional variable range hopping of localized charges (See Fig. S2 in Supplementary Materials). For lightly-doped samples, there is a semiconducting or insulating behaviors observed in the resistivity-temperature dependence[23, 24] but it is unclear whether it is a character of an intrinsic band insulator or a charge localization effect. Our results favor the latter. Our work clearly indicates that there is a true gap opening or complete loss of spectral weight at the Fermi level along the entire underlying Fermi surface so that the lightly-doped samples are insulators.

We note that, while the nodal gap has been reported before in a number of underdoped cuprates[20, 21, 25], our observations are different in an important aspect. It was reported that a nodal gap is observed in the underdoped but superconducting Bi2212 above T_c[20] although there were different reports that no nodal gap is present even in a highly underdoped insulating Bi2212 sample[19, 26]. For the underdoped Bi2212 sample with a T_c near 34 K which was reported to exhibit a nodal energy gap, its resistivity-temperature dependence

shows a good metallic behavior over an entire temperature range[27]. In $(La_{2-x}Sr_x)CuO_4$ system, a nodal gap is reported at a doping level of 0.08 with a T_c at 20 K[21], although transport measurements also indicate that it is already a good metal over a whole temperature range[23, 24]. These results suggest that the nodal gap, the pseudogap and the superconducting gap can occur at the same doping level[20, 21]. In our case of La-Bi2201, it is clear that the nodal gap is competing with the superconducting gap: superconductivity starts to emerge only after the nodal gap disappears. We note that the super-high resolution ARPES measurements enable us to observe clear coherence peaks even in the heavily underdoped samples, thus making it possible to get a precise determination of energy gap. Also, for many samples investigated in the present study, they have the same composition; the doping is slightly tuned by only varying annealing process.

The energy gap observed in the lightly-doped La-Bi2201 samples exhibits a number of characteristics that will be important to reveal its underlying origin of formation. (1). Its momentum dependence is anisotropic, following a d-wave form offset by the nodal gap; (2). It decreases with increasing doping and becomes zero at x$\sim$0.10. In particular, this is a doping level where the three-dimensional antiferromagnetism disappears and superconductivity starts to emerge; (3). For a typical sample with p=0.055, the gap persists up to a temperature of 300 K (Fig. 3) which is close to the pseudogap temperature. The first possibility to check is whether the energy gap can be induced by disorder because disorder can give rise to localization which leads to insulating behaviors. It has been shown theoretically that disorder can drive an insulator-superconductor transition at a critical disorder strength and produce a single particle gap[28]. These aspects bear similarities to our observations of nodal energy gap and an insulator-superconductor transition near x$\sim$0.10. However, it predicts that the nodal gap exists for both the insulating region and the superconducting region, which is inconsistent with our observation that the nodal gap exists only in the insulating samples.

The coincidence of the nodal gap disappearance and the vanishing of the three-dimensional antiferromagnetism near $p\sim$0.10 indicates that long-range antiferromagnetism is closely related with the electronic structure evolution across the insulator-superconductor transition. It is natural to ask whether the static antiferromagnetic order alone can give rise to the energy gap formation in the lightly-doped region. As it is well-known, the presence of static antiferromagnetic order can double the unit cell in real space and reduce the Brillouin

zone in the reciprocal space by half. This would cause band folding that will make the initial "large Fermi surface" and folded Fermi surface cross somewhere in between the nodal and antinodal regions. This is most clearly demonstrated in the electron-doped cuprates[29]. This picture alone cannot explain the gap formation near the nodal region, it cannot explain the anisotropic *d*-wave like gap form either. Very recently it was pointed out by theoretical calculations that the nodal *d*-wave spectrum is robust against strongly fluctuating competing order like antiferromagnetic correlation. But when the antiferromagnetic correlation is strong and the phase has spatial inhomogeneity, a nodal gap can be developed which grows with the antiferromagnetic magnitude[30]. This picture may be able to account for the nodal gap opening in the lightly-doped region. However, the result is obtained in a weak coupling approach and it shows a strong temperature dependence that is different from what we have observed.

In order to understand the electronic characteristics of the lightly-doped region, in addition to the formation of the nodal gap, one needs to pay special attention to the systematic doping evolution of the spectral functions which contains a wealth of information. In particular, we have to consider the emergence of the coherence peak with a slight doping, the coexistence of the coherence peak with a broad hump, and the coordinated evolution of the coherence peak and the hump with doping. These observations were also reported in other copper-oxide compounds[14, 15]. They bear resemblance to the spectra of some one-dimensional materials[31] and bilayer manganite $La_{1.2}Sr_{1.8}Mn_2O_7$[32]. These behaviors can be reasonably explained by the formation of small polarons[15, 31, 33, 34] with electrons dressed by spin excitations or lattice vibrations. The EDC spectra can be explained by Franck-Condon broadening (FCB), in which the quasi-particle coherence peak represents the coherent part of the spectral function whereas the broad hump consists of excited states comprising the incoherent part[15, 31, 33, 34]. This polaron picture can probably account for the lineshape of the photoemission spectra we observed and their doping evolution. However, it does not provide a satisfactory explanation of the energy gap. In a simple polaron picture, the primary coherence peak is expected to stay at the Fermi level although its spectral weight may change with doping[31].

It is intriguing to examine whether the combined effect of strong correlation, antiferromagnetism and electron-phonon interaction can account for all our observations in the lightly-doped La-Bi2201 samples. It is shown by theoretical calculations from the Hubbard

model[35] and the t-J model [36] that antiferromagnetism can enhance the electron-phonon interaction. This enhancement could make the formation of self-trapped polarons much more likely although there is no consensus reached for the critical value of the electron-phonon coupling constant. Once the self-trapped polaron is formed, the spectral weight of the quasiparticle at the Fermi level is reduced to zero[36]. In addition, there are several peaks appeared at higher binding energies as the motion of the charge is strongly coupled with the creation of spin wave excitations and phonons. It is known that doping will suppress the antiferromagnetism and also the electron-phonon interaction[15, 35, 37]. Hence, in the extremely low doping region (like p=0.03 and below) with a very strong antiferromagnetic order, the effective electron-phonon interaction is very strong, those peaks appeared at rather high binding energy and there is no spectral weight at the Fermi level. It may seem like there is a large gap. When doping increases (like p=0.04$\sim$0.08), the peaks would begin to move toward the Fermi level but still without any spectral weight at the Fermi level until the effective electron-phonon interaction reduces below a critical value. In this case, the electron-phonon interaction is just to renormalize the quasiparticle mass with a finite spectral weight at the Fermi level. Our observation of the simultaneous disappearance of the antiferromagnetism and the nodal gap (or lack of spectral weight at the Fermi level) seems to agree quite well with this picture. The excellent fitting of the temperature dependence of resistivity with a variable range hopping model (Fig. S2 in Supplementary Materials) is also quite consistent with the formation of localized ploarons. Another important prediction of the theories[36, 38] is that the momentum dependence of the peaks at higher binding energies follows the same energy dispersion of the quasiparticles without any electron-phonon interaction. Thus the *d*-wave like momentum dependence of the ARPES spectra shown in Fig. 4 can be naturally understood; its implication will be discussed below. We also note that Fig. 4(a-e) shows a rigid energy shift along almost the entire Fermi surface. Any mechanism for the formation of the nodal gap should not modify the Fermi surface. The polaron picture is again a natural candidate for this effect. However, we still need a more quantitative explanation of the spectral lineshape for the insulating regime.

One important question to ask is the relationship between the energy gap observed in the insulating samples (x=0$\sim$0.10) and the pseudogap observed in the underdoped superconducting region (x=0.10$\sim$0.15). In Fig. 4l, for several given momenta, we plotted the energy gap observed in the insulating region (x=0$\sim$0.10) and the pseudogap observed in the

underdoped superconducting region (x=0.10∼0.105). The region with the insulating gap smoothly evolves into the pseudogap region without an abrupt change. In conjunction with the *d*-wave-like gap form, the decrease of the nodal gap as doping increases from 0.04 to 0.10 also reduces the gap value at the antinodal region to about 40 meV that is close to the maximum pseudogap value observed for the superconducting phase[19]. This is the first experimental evidence that has been presented about the continuous increase of the pseudogap at the antinodal region as the system crosses from the superconducting phase to the insulating antiferromagnetic phase. Our result of the *d*-wave-like gap form is qualitatively consistent with the idea that the d-wave-like spin singlet pairing already exists in the insulating parent compound and lightly-doped samples[39]. It is theoretically shown that, even if there is a long range antiferromagnetic order, energy dispersion still has the d-wave-like form along the Fermi surface[40]. However, due to the presence of the antiferromagnetic phase, the electron-phonon interaction is greatly enhanced to create polarons and needs to be considered to account for the spectral lineshape and the nodal gaps we have observed. Since the antiferromagnetic fluctuation and electron-phonon coupling are present well into the higher doping region in spite of their reduced strength[34], one may expect they also play important role in dictating the electronic structure and properties in higher doping regions.

In summary, we have observed a clear insulator-superconductor transition in the La-Bi2201 system near the doping level of ∼0.10, taking advantage of our super-high resolution laser ARPES measurements. In the lightly-doped region below the critical doping ∼0.10, fully-opened gap is observed for all samples along the entire underlying Fermi surface, including the nodal region. The nodal gap gets small with the increase of the doping level and approaches zero at the critical doping p∼0.10 where the three-dimensional antiferromagnetic order vanishes and superconductivity starts to emerge. The spectral property of the nodal gap and the d-wave-like gap form along the underlying Fermi surface in the insulating phase is qualitatively consistent with the idea of having a self-trapped polaron. Hence our results indicate that antiferromagnetic correlation and the strong electron-phonon interaction are important to understand the electronic structure and anomalous physical properties of

cuprates, at least in the underdoped region.

[1] Lee, P. A. Doping a Mott insulator:Physics of high temperature superconductivity. Rev. Mod. Phys. **78**, 17-85 (2006).

[2] Tsuei, C. C. and Kirtley, J. R. Pairing symmetry in cuprate superconductors. Rev. Mod. Phys. **72**, 969-1016 (2000).

[3] Timusk T. & Statt B. The pseudogap in high-temperature superconductors: an experimental survey. Rep. Prog. Phys. **62**, 61-122 (1999).

[4] Bollinger, A. T. Superconductor-insulator transition in $La_{2-x}Sr_xCuO_4$ at the pair quantum resistance. Nature (London) **472**, 458-460 (2011).

[5] Kohsaka, Y. et al. Visualization of the emergence of the pseudogap state and the evolution to superconductivity in a lightly hole-doped Mott insulator. Nature Phys. **8**, 534-538 (2012).

[6] Kawasaki, S. et al. Carrier-concentration dependence of the pseudogap ground state of superconducting $Bi_2(Sr_{2-x}La_x)CuO_{6+\delta}$ revealed by ^{65,66}Cu-nuclear magnetic resonance in very high magnetic fields. Phys. Rev. Lett. **105**, 137002/1-4 (2010).

[7] Liu, G. D. et al. Development of a vacuum ultraviolet laser-based angle-resolved photoemission system with a superhigh energy resolution better than 1 meV. Rev. Sci. Instruments **79**, 023105/1-11 (2008).

[8] Meng, J. Q. et al. Growth, characterization and physical properties of high-quality large single crystals of $Bi_2(Sr_{2-x}La_x)CuO_{6+\delta}$ high-temperature superconductors. Supercond. Sci. Technol. **22**, 045010/1-6 (2009).

[9] Gros, C. et al., Determining the underlying Fermi surface of strongly correlated superconductors, PNAS **103**, 14298-14301 (2006).

[10] Norman, M. R., Randeria, M., Ding H. & Campuzano, J. C. Phenomenology of the low-energy spectral function in high-T_c superconductors. Phys. Rev. B **57**, R11093-R11096 (1998).

[11] Norman, M. R. et al. Destruction of the Fermi surface in underdoped high-T_c superconductors. Nature (London) **392**, 157-160 (1998).

[12] Kanigel, A. et al. Evolution of the pseudogap from Fermi arcs to the nodal liquid. Nature Phys. **2**, 447-451 (2006).

[13] Lee, W. S. et al. Abrupt onset of a second energy gap at the superconducting transition of

underdoped Bi2212. Nature (London) **450**, 81-84 (2007).

[14] Yoshida, T. et al. Metallic behavior of lightly doped $La_{2-x}Sr_xCuO_4$ with a Fermi surface forming an arc. Phys. Rev. Lett. **91**, 027001/1-4 (2003).

[15] Shen, K. M. et al. Missing quasiparticles and the chemical potential puzzle in the doping evolution of the cuprate superconductors. Phys. Rev. Lett. **93**, 267002 (2004).

[16] Hashimoto, M. et al. Doping evolution of the electronic structure in the single-layer cuprate $Bi_2(Sr_{2-x}La_x)CuO_{6+\delta}$: Comparison with other single-layer cuprates. Phys. Rev. B **77**, 094516/1-9 (2008).

[17] Pan, Z. H. et al. Evolution of Fermi surface and normal-state gap in the chemically substituted cuprates $Bi_2Sr_{2-x}Bi_xCuO_{6+\delta}$. Phys. Rev. B **79**, 092507/1-4 (2009).

[18] Ronning, F. et al. Photoemission evidence for a remnant Fermi surface and a d-Wave-Like dispersion in insulating $Ca_2CuO_2Cl_2$. Science **282**, 2067-2072 (1998).

[19] Chatterjee, U. et al. Observation of a d-wave nodal liquid in highly underdoped $Bi_2Sr_2CaCu_2O_{8+\delta}$. Nature Physics **6**, 99-103 (2010).

[20] Vishik, I. M. et al. Phase competition in trisected superconducting dome. PNAS **6**, 18332/ 18337 (2012).

[21] Razzoli, E. et al. Evolution from a nodeless gap to $d_{x^2-y^2}$ form in underdoped $La_{2-x}Sr_xCuO_4$. Phys. Rev. Lett. **110**, 047004 (2013).

[22] Lupi, S. et al. Far-Infrared Absorption and the Metal-to-Insulator Transition in Hole-Doped Cuprates. Phys. Rev. Lett. **102**, 206409 (2009).

[23] Takagi, H. et al., Systematic evolution of temperature-dependent resistivity in $La_{2-x}Sr_xCuO_4$. Phys. Rev. Lett. **69**, 2975-2978 (1992).

[24] Ando, Y. et al. Mobility of the Doped Holes and the Antiferromagnetic Correlations in Underdoped High-Tc Cuprates. Phys. Rev. Lett. **87**, 017001/1-4(2001).

[25] Shen, K. M. et al. Fully gapped single-particle excitations in lightly doped cuprates. Phys. Rev. B **69**, 054503/1-4 (2004).

[26] Yang, H. B. et al., Reconstructed Fermi surface of underdoped $Bi_2Sr_2CaCu_2O_{8+\delta}$ cuprate superconductors, Phys. Rev. Lett. **107**, 047003/1-4(2011).

[27] Sun, X. F. et al., Doping dependence of phonon and quasiparyicle heat transport of pure and Dy-doiped $Bi_2Sr_2CaCu_2O_{8+\delta}$ single crystals, Phys. Rev. B **77**, 094515/1-10(2008).

[28] Bouadim, K. et al. Single- and two-particle energy gaps across the disorder-driven supercon-

ductorCinsulator transition. Nature Physics **7**, 884-889 (2011).

[29] Matsui, H. et al., Angle-resolved photoemission spectroscopy of the antiferromagnetic superconductor $Nd_{1.87}Ce_{0.13}CuO_4$: anisotropic spin-correlation gap, pseudogap, and the induced quasiparticle mass enhancement. Phys. Rev. Lett. **94**, 047005 (2005).

[30] Atkinson, W. A. et al. Robustness of the nodal d-wave spectrum to strongly fluctuating competing order. Phys. Rev. Lett. **109**, 267004 (2012).

[31] Perfetti, L. et al. Mobile small polarons and the Peierls transition in the quasi-one-dimensional conductor $K_{0.3}MoO_3$, Phys. Rev. B **66**, 075107 (2002).

[32] Mannella, N. et al. Nodal quasiparticle in pseudogapped colossal magnetoresistive manganites. Nature (London) **447**, 474-478 (2005).

[33] Rösch, O. et al. Polaronic behavior of undoped High-T_c cuprate superconductors from angle-resolved photoemission spectra. Phys. Rev. Lett. **95**, 227002/1-4(2005).

[34] Zhou, X. J. et al. in *Handbook of High-Temperature Superconductivity: Theory and Experiment*, Chapter 3, edited by J. R. Schrieffer and J. Brooks, (Springer, New York). (2007).

[35] Sangiovanni, G. et al. Electron-phonon interaction and antiferromagnetic correlations. Phys. Rev. Lett. **97**, 046404/1-4(2006).

[36] Mishchenko, A. and Nagaosa, N. Electron-phonon coupling and a polaron in the t-J model: From the weak to the strong coupling regime. Phys. Rev. Lett. **93**, 036402/1-4(2004).

[37] Zhou, X. J. et al. Universal nodal Fermi velocity. Nature (London) **423**, 398 (2003).

[38] Bonca, J. et al. Spectral properties of a hole coupled to optical phonons in the generalized t-J model. Phys. Rev. B **77**, 054519/1-4 (2008).

[39] Anderson, P. W. The resonating valence bond state in La_2CuO_4 and superconductivity. Science **235**, 1196-1198 (1987).

[40] Lee, T. K., Ho, C. M. and Nagaosa, N. Theory for slightly doped antiferromagnetic Mott insulators, Phys. Rev. Lett. **90**, 67001/1-4 (2003).

Supplementary Information is linked to the online version of the paper.

Acknowledgements We acknowledge helpful discussions with Prof. Chandra Varma. XJZ thanks the funding support from NSFC (Grant No. 11190022) and the MOST of China (Program No: 2011CB921703 and 2011CB605903).

Author Contributions X.J.Z.and Y.Y.P. proposed and designed the research. Y.Y.P.,

J.Q.M., D.X.M., J.F.H., L.Z., G.D.L., X.L.D., S.L.H., J.Z., X.Y.W., Q.J.P., Z.M.W., S.J.Z., F.W., C.T.C., Z.Y.X. and X.J.Z contributed to the development and maintenance of Laser-ARPES system. Y.Y.P. prepared and characterized the samples with help from J.Q.M., Y.W. and X.L.D.. Y.Y.P. carried out the experiment and data analysis with the assistance from J.Q.M., D.X.M., J.F.H., L.Z., G.D.L., S.L.H. and X.J.Z.. X.J.Z., Y.Y.P. and T.K.L. wrote the paper.

Author Information Correspondence and requests for materials should be addressed to X.J.Z. (XJZhou@aphy.iphy.ac.cn).

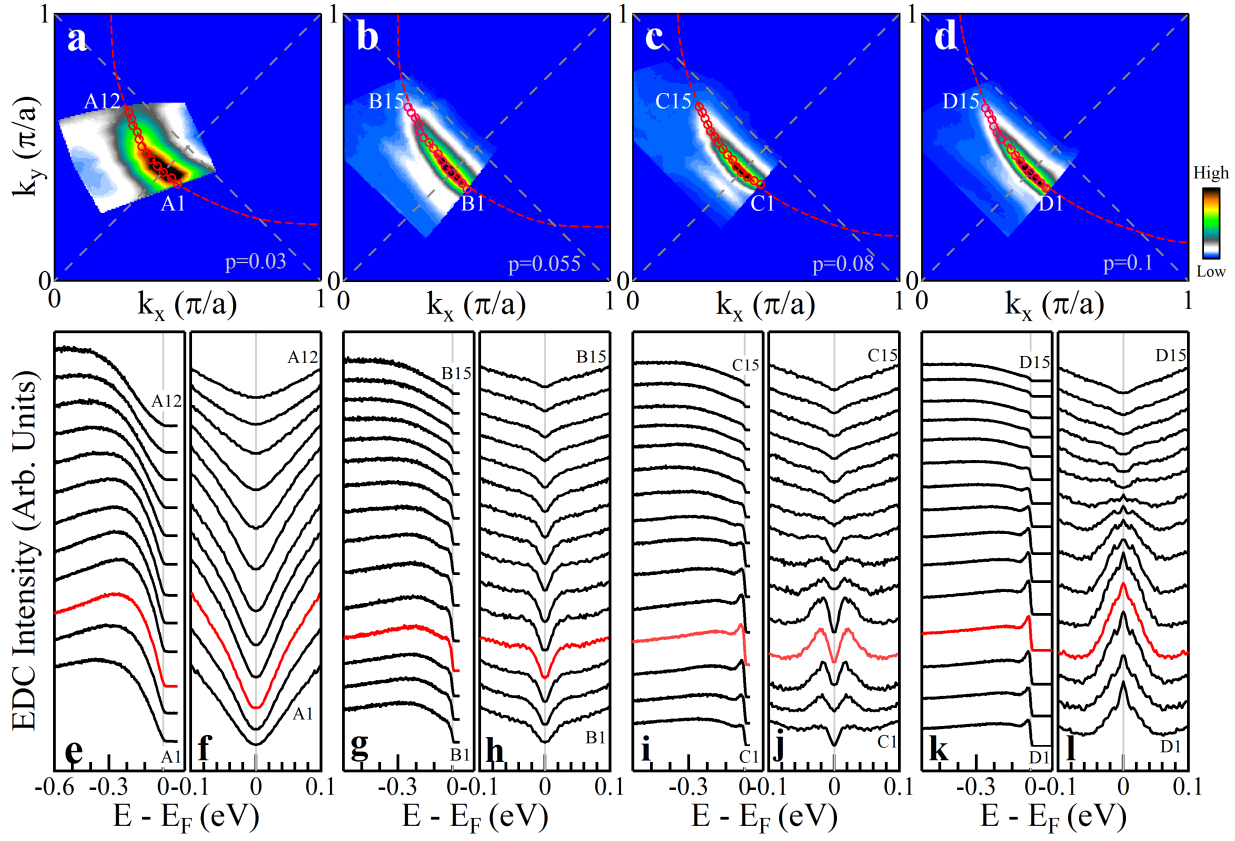

FIG. 1: Observation of the nodal gap in lightly doped La-Bi2201 samples. (a to d) The momentum distribution of the spectral weight integrated within a [-10meV,10meV] energy window around E_F for La-Bi2201 samples with different doping levels p of 0.03 (a), 0.055 (b), 0.08 (c) and 0.10 (d). The data were taken at a temperature of 20 K. The location of the "underlying Fermi surface" is labeled by red empty circles and the red dashed lines are obtained by tight-binding fits to the circles which serves as a guide to the eyes. The photoemission spectra (energy distribution curves, EDCs) along the "underlying Fermi surface" are shown in (e), (g), (i) and (k) for the doping levels of 0.03 (e), 0.055 (g), 0.08 (i) and 0.10 (k), respectively. The corresponding symmetrized EDCs are shown in (f), (h), (j) and (l). Red lines indicate the EDCs and symmetrized EDCs along the (0,0)-(π,π) nodal direction. We paid special attention to avoid any charging effect due to the insulating behaviors of these lightly-doped samples. We varied the photon flux over a large range and observed little change in the measured EDCs.

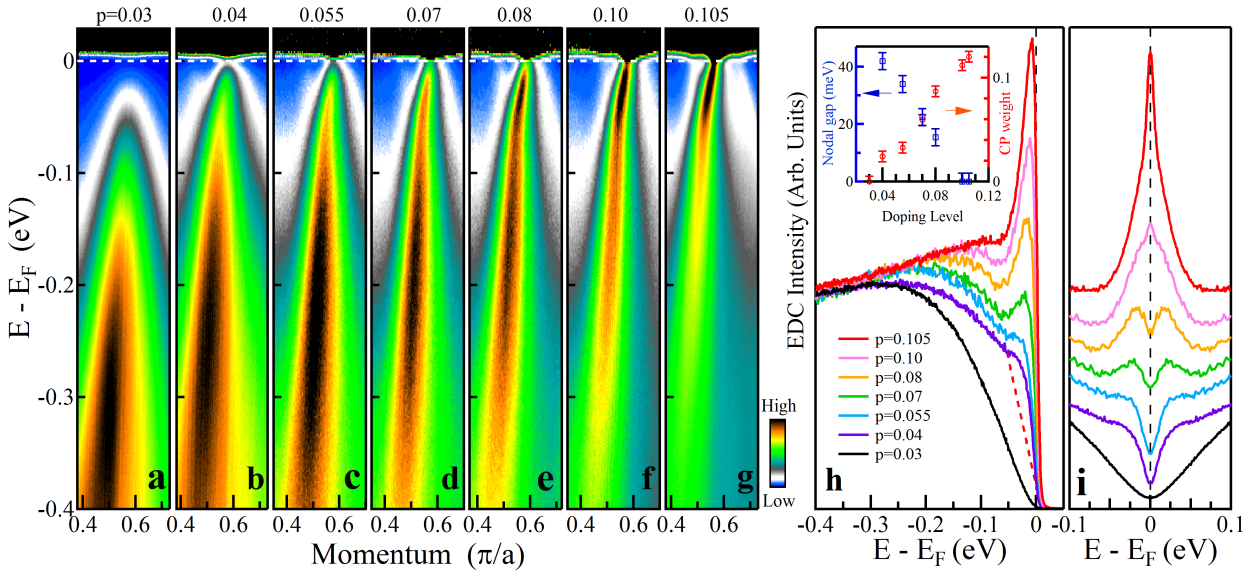

FIG. 2: Doping evolution of the nodal gap in lightly-doped La-Bi2201 samples. (a to g) Band structures measured along the nodal direction for the La-Bi2201 samples with different doping levels p of 0.03 (a), 0.04 (b), 0.055 (c), 0.07 (d), 0.08 (e), 0.10 (f) and 0.105 (g). The data were taken at a temperature of ∼15 K and were divided by the Fermi distribution function to highlight the gap opening near the Fermi level. (h) shows the original EDCs on the "underlying Fermi surface" along the nodal direction; the corresponding symmetrized EDCs are shown in (i). The top-left inset in (h) shows the doping dependence of the nodal gap (blue empty squares) and the coherence peak (CP) spectral weight (red empty circles). The nodal gap is obtained by taking the peak position of the symmetrized EDCs in (i). The coherence peak spectral weight (CP weight) is defined by the ratio between the peak area and the overall spectral weight integrated over the [-0.4eV,0.03eV] energy window. The coherence peak area is obtained by subtracting a linear background (red dashed line) as illustrated in (h) for the EDC of the p=0.04 sample.

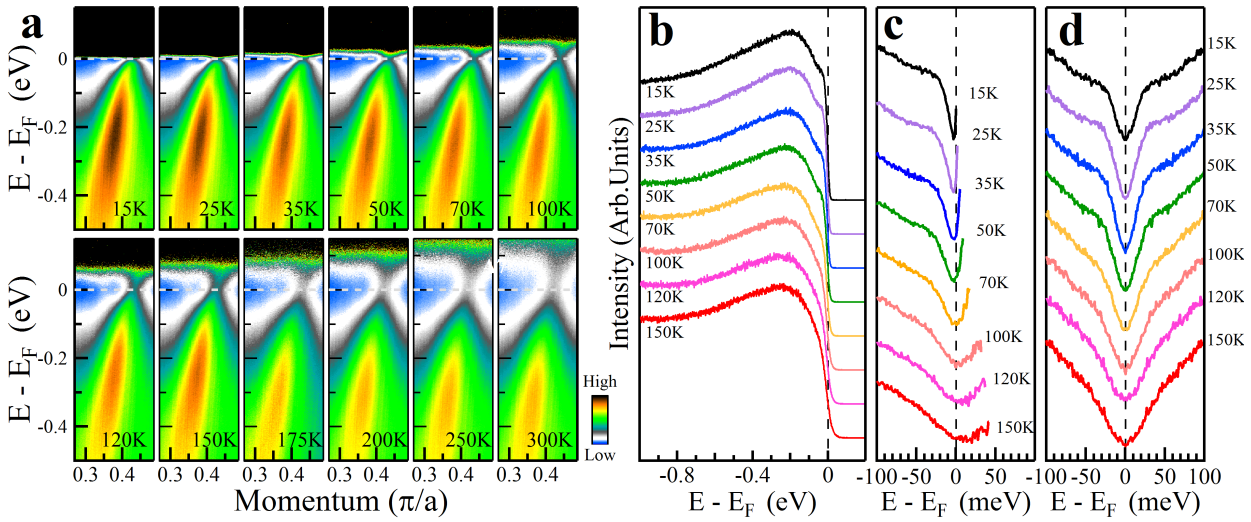

FIG. 3: Temperature dependence of the nodal gap. (a) Band structure of the La-Bi2201 sample with a doping level of p=0.055 measured along the nodal direction at different temperatures. The data have been divided by the corresponding Fermi distribution functions to highlight the energy gap and the features above the Fermi level. (b) Original EDCs at the underlying Fermi momentum at different temperatures. (c). Corresponding EDCs after being divided by the Fermi distribution functions. (d). Symmetrized EDCs obtained from (b). Sample ageing has been checked by cycling temperature and the data are reproducible during the process.

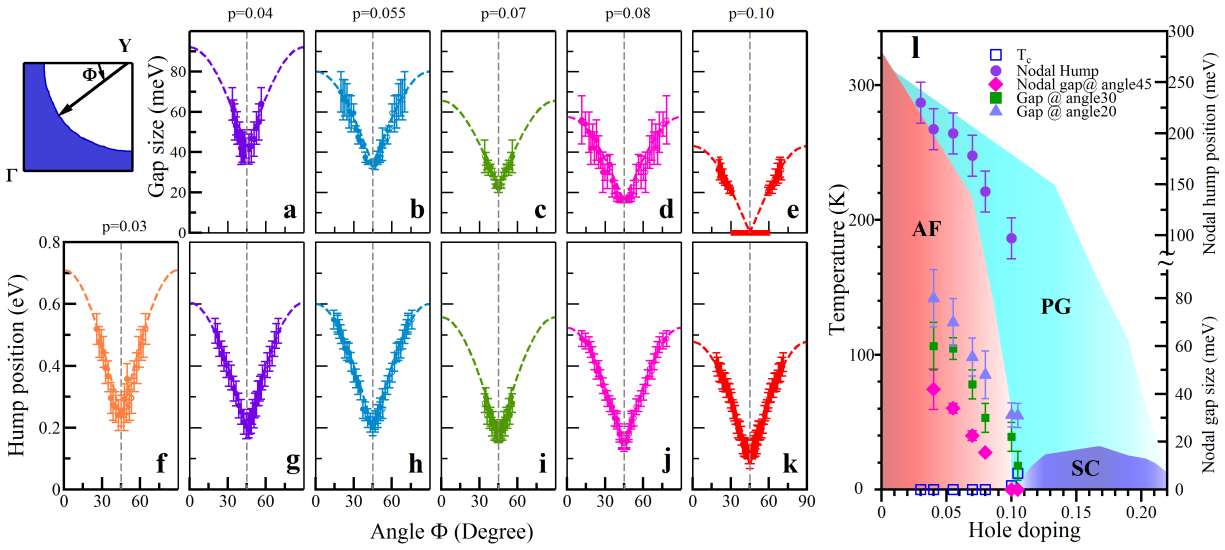

FIG. 4: Momentum dependence of the energy gap and its evolution with doping in lightly-doped La-Bi2201 samples measured at 20 K. (a-e) show the momentum dependence of the energy gap with different doping levels p of 0.04 (a), 0.055 (b), 0.07 (c), 008 (d) and 0.10 (e). The Φ angle is defined in the top-left inset with Φ=45 degrees corresponding to the nodal direction. The gaps are symmetrized with respect to the nodal direction for better visualization (empty circles). The dashed lines depict the offset d-wave form $\Delta=\Delta_0\cos(2\Phi)+\Delta_N$ with the offset Δ_N corresponding to the nodal gap. (f to k) Momentum evolution of the hump for La-Bi2201 samples with different doping levels p of 0.03 (f), 0.04 (g), 0.055 (h), 0.07 (i), 0.08 (j) and 0.10 (k). The dashed lines represent a form of $P_h=P_{h0}\cos(2\Phi)+P_{hN}$ with P_{hN} representing the hump position along the nodal direction. (l) Phase diagram of La-Bi2212 system. It shows the three-dimensional antiferromagnetic region defined by T_N, superconducting region defined by T_c and the pseudogap region defined by T^*. T_N and T^* are reproduced from the previous NMR measurements[6]. T_c is determined from our magnetization and resistivity measurements. The doping dependence of the nodal gap size (pink diamond) and the nodal hump position (blue circles) are plotted. The energy gap away from the nodal direction, with Φ=30 degrees (green solid squares) and 20 degrees (blue solid triangles) are also plotted. We note that at $p\sim$0.10, the nodal gap goes to zero, the three-dimensional antiferromagnetism vanishes (T_N goes to zero), and superconductivity starts to emerge.